

# Cepheid theoretical models and observations in HST/WFC3 filters: the effect on the Hubble constant $H_0$

Giuliana Fiorentino<sup>1,2\*</sup>, Ilaria Musella<sup>3</sup> and Marcella Marconi<sup>3</sup>

<sup>1</sup>*INAF-Osservatorio Astronomico di Bologna, via Ranzani 1, 40127, Bologna, Italy*

<sup>2</sup>*Dipartimento di Astronomia, Università di Bologna, via Ranzani 1, 40127, Bologna, Italy*

<sup>3</sup>*INAF, Osservatorio Astronomico di Capodimonte, via Moiariello 16, 80131, Napoli, Italy*

Accepted XX. Received XX; in original form 2013 April 29

## ABSTRACT

We present a complete theoretical scenario for classical Cepheids in the most commonly used HST/WFC3 filters, going from optical (F555W, F606W and F814W) to near-infrared (F160W) bands. The importance of such a study is related to the recent release of new classical Cepheids observed with HST/WFC3 in 8 distant galaxies where SNIa are hosted. These observations have posed sound constraints to the current distance scale with uncertainties on the Hubble constant  $H_0$  smaller than 3%. Our models explore a large range of metallicity and Helium content, thus providing a robust and unique theoretical tool for describing these new and future HST/WFC3 observations. As expected, the Period–Luminosity (PL) relation in F160W filter is linear and slightly dependent on the metallicity when compared with optical bands, thus it seems the most accurate tool to constrain extragalactic distances with Cepheids.

We compare the pulsation properties of Cepheids observed with HST/WFC3–IR with our theoretical scenario and we discuss the agreement with the predicted Instability Strip for all the investigated galaxy samples including the case of NGC4258.

Finally, adopting our theoretical F160W PL relation for  $Z=0.02$  and  $\log P \gtrsim 1.0$ , we derive new distance moduli. In particular, for NGC 4258, we derive a distance modulus  $\mu_0 = 29.345 \pm 0.004$  mag with a  $\sigma = 0.34$  mag, which is in very good agreement with the geometrical maser value. Moreover, using the obtained distance moduli, we estimate the Hubble constant value,  $H_0 = 76.0 \pm 1.9$  km s<sup>-1</sup> Mpc<sup>-1</sup> in excellent agreement with the most recent literature values.

**Key words:** galaxies: spiral — stars: distances — stars: variables: Cepheids

## 1 INTRODUCTION

Major improvements in the classical Cepheid extragalactic distance scale have been obtained in the last 20 years thanks to the Hubble Space Telescope (HST) observations of a number of galaxies containing both Cepheids and SNIa out to distances of  $\sim 25$  Mpc (Freedman & Madore 2010). In the literature, the Cepheid period–luminosity (PL) relation is often adopted in the optical bands (V and I) and calibrated using the relation of the Large Magellanic Cloud (LMC) Cepheid sample. However, the optical PL relations suffer from metallicity effects and, in the case of metal poor samples ( $Z < 0.01$ ), nonlinearity (see e.g. Caputo et al. 2000). Moreover, the zero point depends on the assumed LMC distance and the slope is traditionally assumed to be universal, in spite of several investigations that find a non negligible metallicity effect (Sakai et al.

2004; Tammann et al. 2003; Bono et al. 2010; Ngeow et al. 2012). The LMC has the advantage of being quite near (about 50 Kpc), so that its distance has been measured using different primary distance indicators (RR Lyrae, Tip of the Red Giant Branch, Red–Clump, etc, Fiorentino et al. 2011; Walker 2012; Laney et al. 2012; Haschke et al. 2012; Marconi et al. 2012). Moreover, a large sample of Cepheids has been released by the micro–lensing experiments carried out in this galaxy. In particular, the last catalogue from OGLE III includes more than 3,000 objects (Soszyński et al. 2008). However, the HST galaxies with SNIa typically have metallicities much higher than the LMC ( $Z > 0.02$  compared to  $Z = 0.008$ ). The metallicity dependence of the PL relation has been largely debated in the literature both from the theoretical and the observational point of view, even if a general consensus has not been achieved yet (e.g. Kennicutt et al. 1998; Caputo et al. 2002; Sakai et al. 2004; Macri et al. 2006; Fiorentino et al. 2002; Marconi et al. 2005; Bono et al. 2008, 2010; Romaniello et al. 2008, and

\* E-mail: giuliana.fiorentino@oabo.inaf.it

references therein). Nonlinear convective pulsation models also suggest a non negligible dependence on the Helium content (Fiorentino et al. 2002; Marconi et al. 2005).

Moreover, there are suggestions that the optical PL relations in the SMC and LMC are not linear over the whole period range, showing a change in the slope at periods around 10 days (see Sakai et al. 2004; Ngeow et al. 2005; Marconi et al. 2005, for details). This does not seem to be the case for Galactic Cepheids (Tammann et al. 2003). Although further investigations on the nonlinearity are needed for definitive claims, LMC might not be the ideal sample to set both the slope and the zero-points of optical PL relations.

On the other hand, observational and theoretical investigations suggest that in the near-infrared (NIR) bands (J and K), that are also much less affected by the reddening, both the chemical composition and nonlinearity effects are significantly reduced (Bono et al. 1999a; Marconi et al. 2005; Fiorentino et al. 2007; Freedman et al. 2012). Another advantage of the NIR bands is that, given the small pulsation amplitudes in these filters, only one epoch is sufficient to derive accurate mean magnitudes (with an error of about 0.05 mag), once detections and periods are available from optical data (Soszyński et al. 2005; Scowcroft et al. 2011; Ripepi et al. 2012; Inno et al. 2013). In this context, Riess et al. (2011) decided to follow-up with the WFC3-IR camera on board HST the Cepheid samples discovered in seven SNIa hosting galaxies previously observed in the optical bands by using WFPC2 and/or ACS@HST (Riess et al. 2009a,b). To further minimize the uncertainties in the zero point due to the metallicity difference among LMC and metal-rich galaxies, Riess et al. (2011) have chosen NGC4258 as anchor for the Cepheid PL relation. In fact, this galaxy has a very accurate geometrical distance estimate,  $d=7.2\pm 0.5$  Mpc (or  $\mu_0 = 29.29_{-0.16}^{+0.14}$  mag Herrnstein et al. 2005), based on the analysis of its H<sub>2</sub>O maser emission. To remove the reddening uncertainty, these authors adopt a Wesenheit relation based on the combination of the three filters *V*, *I*, and *F160W* (see Riess et al. 2011, for details), in the assumption that the extinction law is universal.

To properly compare our set of nonlinear convective pulsation models (see Marconi et al. 2005; Bono et al. 2008, and references therein) to these recent observations we have transformed the whole framework in WFC3/HST filters. The paper is organised as follows. Section 2 briefly describes the theoretical framework and its physical ingredients. The multi-wavelength relations connecting periods with magnitudes and colours are presented in Section 3. In Sections 4 and 5 we discuss a comparison between theory and the Cepheid samples observed in SNIa hosting galaxies. In Section 6 we give new estimates of the distance moduli for these galaxies and, correspondingly, a new value for the Hubble constant  $H_0$ . The conclusions close the paper.

## 2 PULSATION MODELS AND TRANSFORMATIONS

In the last 15 years, we have computed an extended set of pulsating models for masses representative of Classical Cepheids ( $3 \lesssim M/M_\odot \lesssim 12$ ) using a code originally de-

veloped by Stellingwerf (1978) and subsequently adapted to Classical Cepheids by Bono et al. (1999b,a). A large range of input physical parameters has been explored in order to investigate their effect on the Cepheid intrinsic properties (Bono et al. 2000; Fiorentino et al. 2002; Marconi et al. 2005; Fiorentino et al. 2007; Marconi et al. 2010). In particular, the adopted metallicities range from  $Z=0.0004$  to  $Z=0.04$ , while the Helium content (depending on the assumption on the  $\Delta Y/\Delta Z$  ratio) ranges from 0.24 to 0.34.

With this set of nonlinear pulsational models we predict both the red and the blue boundaries of the classical instability strip (IS) in the Hertzsprung–Russel diagram ( $\log L/L_\odot$  vs  $\log T_{eff}$ ), for each assumed chemical composition. We also build a synthetic stellar population filling the predicted IS with masses in the range  $3 - 12 M_\odot$  and with an initial mass function that follows the relation  $m^{-3}$ . Adopting theoretical evolutionary prescriptions, we can associate to each synthetic stellar mass a luminosity given by a canonical<sup>1</sup> Mass–Luminosity relation whereas the effective temperature is randomly extracted within the IS for a given luminosity level.

These synthetic Cepheid distributions can be transformed into the WFC3/HST photometric system. To this aim, we use the bolometric corrections for both UVIS and IR channels at WFC3/HST carefully computed by S. Cassisi and A. Pietrinferni (priv. comm.). In the following we focus on the most commonly used filters, i.e. F555W (narrow V), F606W (wide V), F814W (wide I) and F160W (wide H). The transformed scenario in the remaining filters is available upon requests. To transform theoretical luminosity and effective temperature into magnitudes and colours we have assumed an updated value for the solar bolometric magnitude  $M_{bol,\odot} = 4.77$  mag (S. Cassisi, priv. comm.). Through regression of these synthetic populations we can finally derive multi-wavelength relations, such as the PL, the PL–Colour (PLC) and the Wesenheit relations.

## 3 THEORETICAL PL AND WESENHEIT RELATIONS

In this section we analyse the properties of the theoretical PL, PLC and Wesenheit relations in the WFC3/HST photometric system with particular attention to the NIR filters, given the increasing role played by both space and ground-based NIR facilities.

We derive the linear PL relations for the whole set of available chemical compositions whose coefficients are reported in Table 1. As expected, these relations become steeper and tighter when passing from optical (F555W) to NIR (F160W) bands with the scatter being reduced by a factor 2. These results confirm that NIR PL relations provide more accurate results than the optical ones, as found recently for the LMC Cepheids (Soszyński et al. 2008; Ripepi et al. 2012; Inno et al. 2013). This finding is further supported by the significant reduction of the reddening effect in these bands, as the ratio between the total to selective extinction decreases of about a factor 5 going from optical

<sup>1</sup> The canonical Mass–Luminosity relation is based on evolutionary models without core over-shooting and mass-loss, as discussed in Bono et al. (2000).

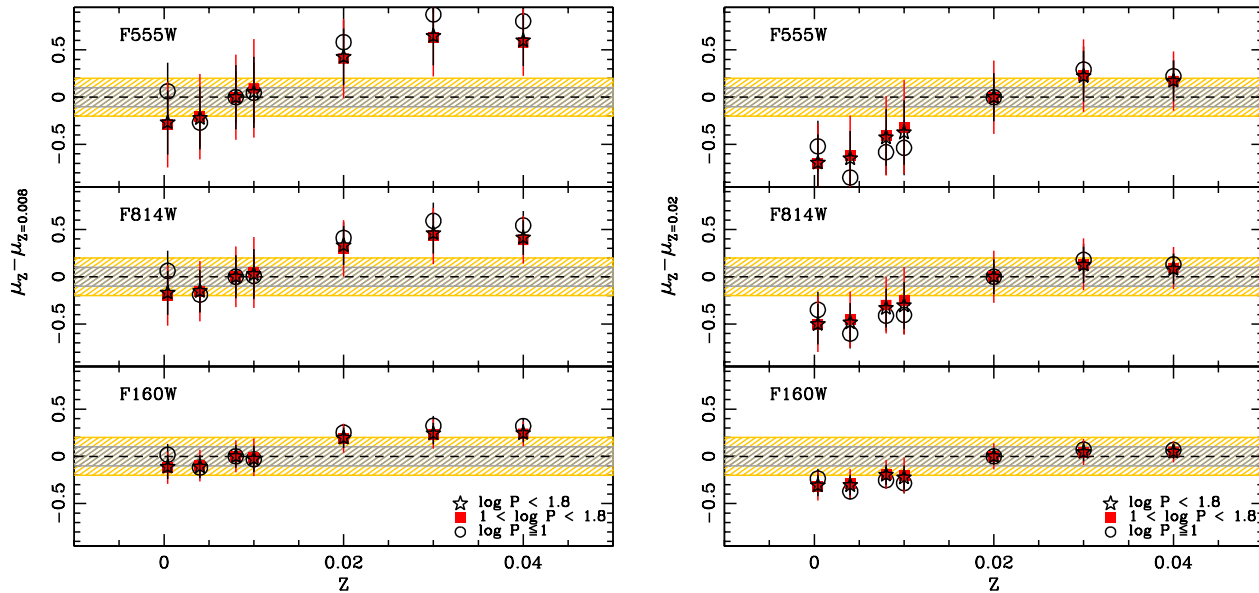


**Figure 1.** Difference between the theoretical distance moduli obtained for each selected metallicity and the corresponding value at  $Z=0.008$  (left) and  $Z=0.02$  (right). This effect is estimated using “broken linear” PL relations in three filters, as labeled in the panels. Grey and light orange regions define 0.1 and 0.2 magnitude range and correspond to errors at the level of 5% and 10% in the final value of the Hubble constant  $H_0$ . Different period ranges, namely  $\log P \leq 1$  (open circles),  $\log P < 1.8$  (open stars) and  $1 < \log P < 1.8$  (red squares) are shown.

to NIR filters ( $R_{F555W} \sim 3.06$  and  $R_{F160W} \sim 0.41$ , derived from Cardelli et al. 1989).

Given the quoted non linearity of the optical PL relations, at least for metallicity typical of the Magellanic Clouds, we derive the coefficients of both the quadratic relations and the linear ones (“broken linear” PL) for periods shorter and longer than 10 days (see Table 2). As expected, with the exception of the very low-metallicity case ( $Z=0.0004$ ), the coefficient of the quadratic term increases by decreasing the metallicity, but the effect is almost removed in the NIR bands.

Since a general consensus on the chemical composition effect on PL relations has not been achieved yet, the metallicity dependence contribution to the final error budget on the extragalactic distance scale is not uniquely quantified. In this context, on the basis of the relations derived in this paper, we provide new constraints to the metallicity effect.

In Fig. 1, by using our synthetic Cepheid samples, we show the predicted differential distance moduli relative to the reference model set with metallicity  $Z=0.008$  (LMC) and  $Z=0.02$  (sun) as a function of the metal content. The distance moduli are obtained with “broken linear” PL relations in the labelled filters. We have distinguished three different period ranges.

As expected, the effect is more significant in the optical filters. Moreover, inspection of this figure suggests that the adoption of the correct reference metallicity is crucial for a significant reduction of the final error in the extragalactic distance scale. In particular, for the supersolar metallicities of the HST galaxies, the adoption of PL relations for solar metallicity reduces the error due to the metallicity effect to few percent. This evidence supports the use of PL relations calibrated on NGC 4258 as adopted by Riess et al.

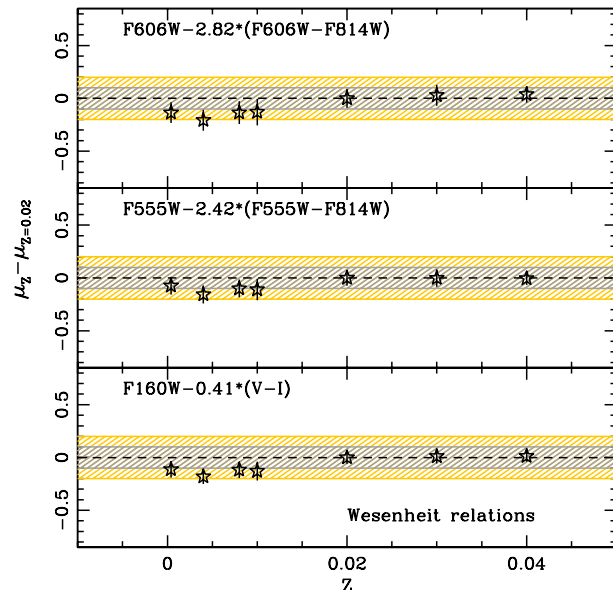


**Figure 2.** As in Fig. 1, but using the Wesenheit relations for the three colour combinations labeled in literature and using as reference the solar-like metallicity  $Z = 0.02$ .

(2011). Considering this result and the period range typical of these extragalactic Cepheid samples (see below), in the following, we adopt the theoretical PL relations for  $Z=0.02$  and  $Y=0.28$  derived for  $\log P > 1$ .

One of the most commonly used tool to derive

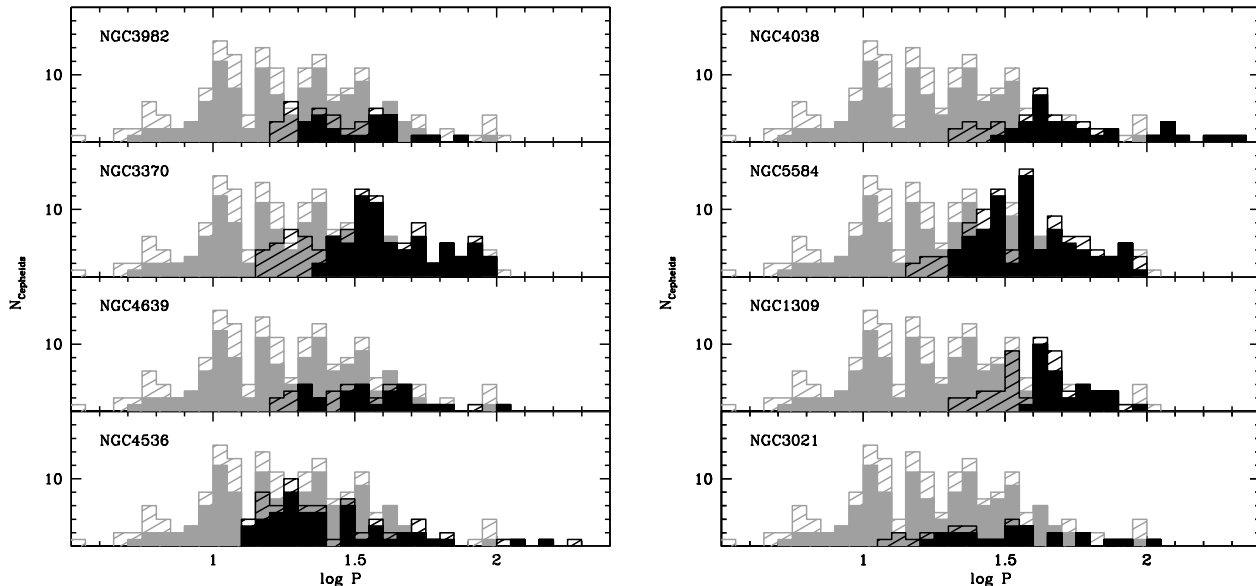


**Figure 3.** Period distributions of the eight host galaxy (black) compared to NGC4258 (grey). The name of the galaxy is labeled in each panel. The shadow regions are the whole Cepheid sample, the filled regions represent the *good* Cepheids used by Riess et al. (2011).

Cepheid distances is the Wesenheit relation (Madore 1976; Fiorentino et al. 2007; Bono et al. 2008; Fiorentino et al. 2010). This formulation has the advantage to be reddening-free by construction and to include a colour term, and in turn the temperature information, for each individual star, defining a very tight relation. In Table 3 we show some of the classical formulations together with the new recent one that combines Johnson-Cousin optical bands and the NIR ones from WFC3/HST photometric system (Riess et al. 2009a, 2011). These relations have been derived using the following extinction coefficients:  $R_{F160W}=0.41$ ,  $R_{F814W}=1.79$ ,  $R_{F606W}=2.78$  and  $R_{F555W}=3.06$  from Cardelli et al. (1989). The predicted intrinsic dispersions are very small, as well as the metallicity effects, making these relations powerful tools for accurate distance determinations.

In Fig. 2 we show the predicted differential distance moduli relative to the reference model set with metallicity  $Z=0.02$  (sun) as a function of the metal content obtained using the Wesenheit relations. This Figure show that the metallicity effect with such relationships is very small, i.e.  $\leq 0.2$  mag or  $\leq 10\%$  in the final value of the Hubble constant  $H_0$ .

#### 4 COMPARISON WITH THE WFC3@HST CEPHEID SAMPLE

As we discussed in the introduction, one of the aims of this paper is the comparison of our pulsation framework with the large Cepheid sample recently observed in NGC4258 and in 8 far SNIa host galaxies with WFC3@HST (Riess et al. 2011). In order to provide new, solid, constraints to the Hubble constant  $H_0$ , Riess et al. (2011) classified Cepheids in each galaxy as *good* or *rejected* through a sigma-clipping (at  $2.5\sigma$ ) rejection criterion with respect to the F160W-PL relation

defined for NGC4258 Cepheids (see Riess et al. 2011, for details).

Table 4 shows the global properties of these galaxies, namely the galaxy ID, the number of total vs *good* Cepheids observed in each galaxy, the mean Cepheid metallicity, the SNIa apparent magnitude and their distance modulus. For each Cepheid, coordinates, period, F160W magnitude and V-I colour are available in Riess et al. (2011). Only for few galaxies (NGC4258, NGC3370, NGC3021 and NGC1309) optical (V, I) individual magnitudes are also at disposal in the literature (Macri et al. 2006; Riess et al. 2009a,b).

##### 4.1 The Cepheid period distributions

In Fig. 3, we plot the comparison among the period distributions of the various galaxies, including the anchor galaxy NGC4258. As well known, the Cepheid samples observed by HST in very distant galaxies are affected by an observational bias both at the short and long-period end of the PL relation due to the limited observational time baseline (see e.g. Freedman et al. 2001, and references therein).

Inspection of Fig. 3 confirms that only for the anchor galaxy NGC4258 periods cover the short range (Macri et al. 2006), whereas for all the others the period distribution span a quite similar range ( $\sim 12$ – $100$  d), with a few significantly ultra long period Cepheids in NGC4536 and NGC4038 (Fiorentino et al. 2012).

##### 4.2 The Cepheid Instability Strip and F160W-PL relation

In this section, we compare our pulsation theoretical predictions to the observations. In Fig. 4 (left panel) we show the theoretical IS compared with the Cepheid distribution in NGC4258 in the magnitude (F160W) vs colour (V-I)

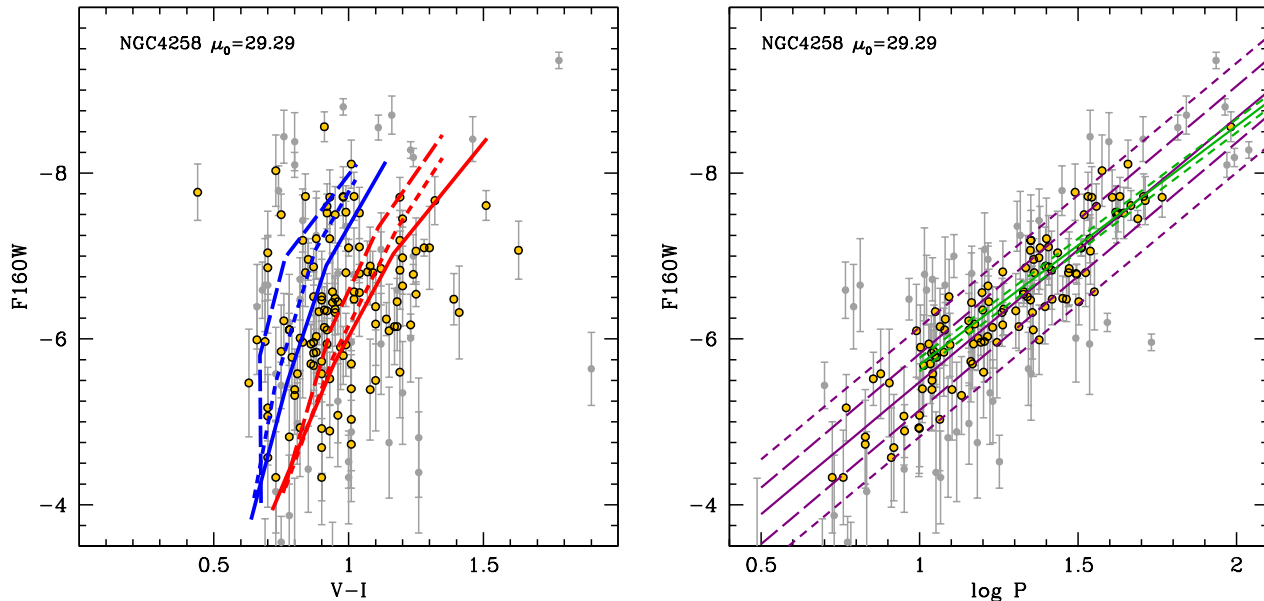


**Figure 4.** –*Left*– Comparison between the observed magnitude–colour distribution (F160W, V–I) of NGC4258 Cepheids and the theoretical boundaries of the pulsation Instability Strip for three different assumptions on the chemical composition:  $Z=0.02;Y=0.28$  (solid),  $Z=0.02;Y=0.31$  (dashed) and  $Z=0.008;Y=0.25$  (long dashed). Orange and grey symbols have been used for good and rejected observed Cepheids, respectively. –*Right*– The same as in the left panel but in the F160 vs  $\log P$  plane. In this panel, we also show the theoretical ( $Z=0.02, Y=0.28$  and  $\log P > 1$ ; dark green solid line) and the observed (purple solid line) F160W–PL relation together with their confidence line (dashed for the whole Cepheid sample and long-dashed for the good ones).

plane. The theoretical ISs for fundamental pulsators are shown for three selected chemical compositions: the solar-like  $Z=0.02;Y=0.28$ , the Helium enriched  $Z=0.02;Y=0.31$  and the LMC-like  $Z=0.008;Y=0.25$ . We assume the distance modulus  $\mu_0 = 29.29$  mag by Herrnstein et al. (2005) and the extinction values by Schlafly & Finkbeiner (2011, see columns 7–8–9 in Table 4). We use different symbols to indicate *good* (light orange dot) and rejected (grey dot) Cepheids. We note that the observed Cepheids show a significantly larger spread than predicted by pulsational models for the solar composition (solid lines). Increasing the Helium abundance, the IS boundaries (dashed lines) move towards hotter effective temperatures (bluer colours). A still larger effect is found for metal-poor LMC-like Cepheid IS boundaries (long-dashed lines). In any case, on average, the colour distribution of Cepheids in NGC4258 seems to be better reproduced by the two model sets with  $Z=0.02$ .

This occurrence is still evident when moving to the NIR PL (right panel of Fig. 4), where pulsation models predict a very narrow and linear relation (dark green lines). This prediction is well supported by recent NIR observations of Cepheids in the LMC and in our Galaxy (Ripepi et al. 2012; Inno et al. 2013; Freedman et al. 2012). From these observations, it is evident that, for wavelength going from  $\sim 1.2$  (J) to 3.6 (mid IR) micron (Scowcroft et al. 2011; Monson et al. 2012), the measured scatter of the PL relation is always less than  $\sim 0.12$  mag. Instead, a linear regression of all the data in right panel of Fig.4 (purple lines) provides a  $\sigma_{PL} = 0.65$  mag. From a further inspection of this Figure, we also note that theoretical models predict a flatter slope ( $\beta_{(Z=0.02;Y=0.28)} = -2.88$ ) than observed ( $\beta_{(NGC4258)} =$

$-3.24$ ) and a larger zero point ( $\alpha_{(Z=0.02;Y=0.28)} = -2.81$  vs  $\alpha_{(NGC4258)} = -2.20$ ).

In Figs 5–6 (left panel) we show the CMD location of Cepheids for each HST sample. Also for these galaxies, we notice a large spread in the observed distributions when compared with the predicted IS boundaries. Moreover, the Cepheid location is on average bluer and brighter than theoretical predictions, with the effect increasing for more distant galaxies. These blue colours have been already pointed out by Tammann & Reindl (2012) for the *extreme* cases of NGC1309 and NGC3021 when compared with Galactic Cepheids. Our pulsational framework suggests very blue colours only for very metal-poor and Helium enriched environments. However, a large variation in the chemical abundance is not supported by recent estimates of the mean metallicity [O/H] in each galaxy (see column three of Table 4). We notice that an overestimate of the reddening can not be the culprit for these blue colours, because the same trend is observed even if we do not account at all for the Galactic extinction. In the right panel of the Figs 5–6, we show the F160W PL distribution for each galaxy. As in the case of NGC4258, in spite of the large spread of these distributions, the agreement with theoretical F160W PL relations is quite satisfactory in particular for *good* Cepheids (black symbols).

The puzzling colour/magnitude behaviour shown by Cepheids could depend on the well known difficulties to perform accurate stellar photometry in crowded distant galaxies. This problem worsens as the distance increases. In particular, a possible systematic effect can be related to the blending from unresolved nearby companions (see e.g. Stetson et al. 1998; Chavez et al. 2012, and references

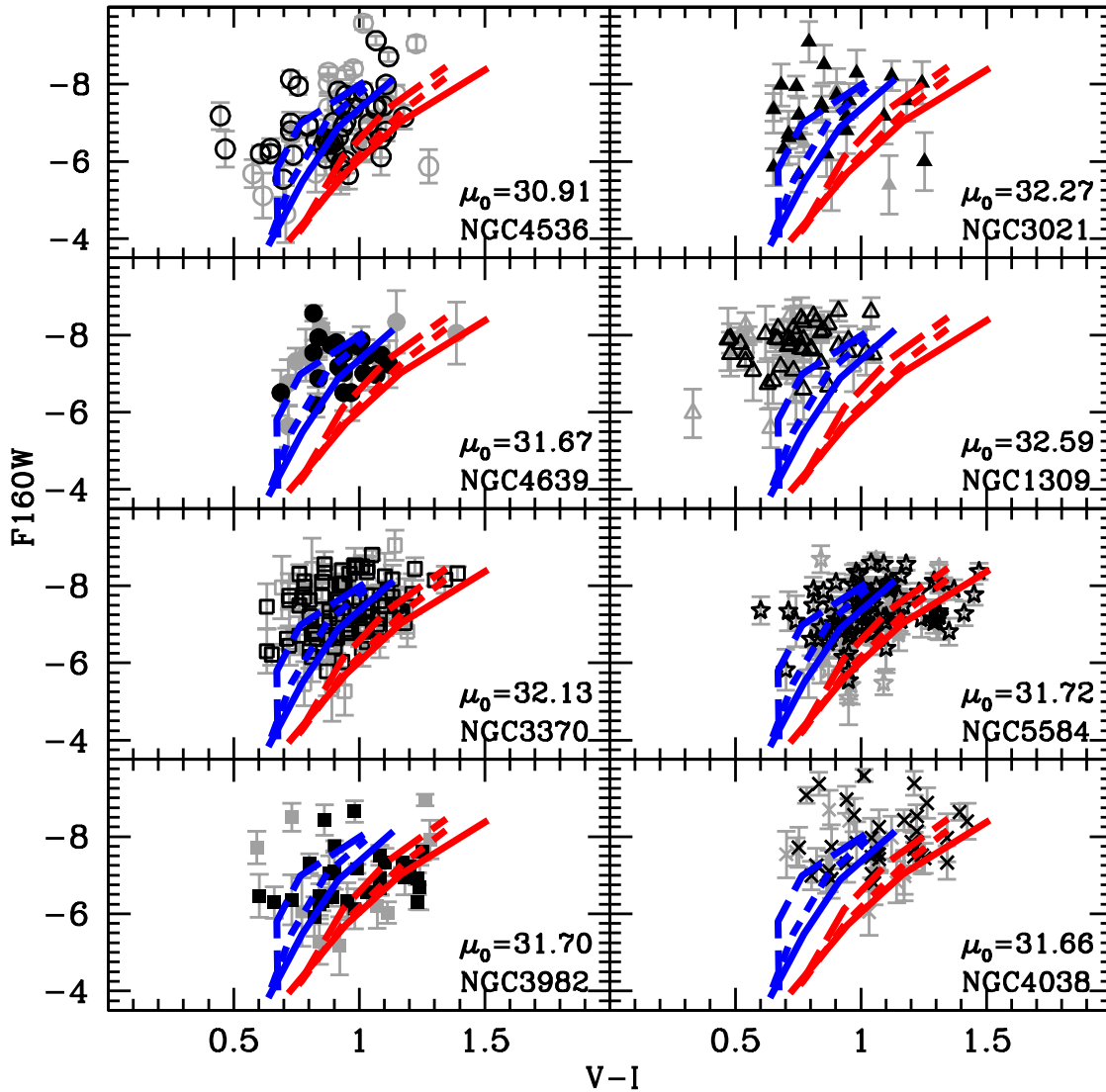


**Figure 5.** The same comparison as in Fig. 4 (left), for each galaxy of the sample. In this case, black and grey symbols represent good and rejected Cepheids as selected in Riess et al. (2011), respectively.

therein) that might produce the observed shift to the hotter and slightly brighter region of the CMD.

## 5 COMPARISON WITH THE ACS@HST CEPHEID SAMPLE

In this Section we focus on the comparison between our theoretical scenario and the properties of Cepheids detected in NGC4258, NGC1309, NGC3021 and NGC3370. For these galaxies individual Johnson V, I magnitudes have been also derived from observations in the F555W and F814W filters of the WFC@ACS on board HST (Macri et al. 2006; Riess et al. 2009a,b).

In Fig. 7 (left panel) we show a comparison between the observations and the theoretical boundaries of the ISs

for fundamental pulsators, for the three chemical compositions adopted in Figs 5-6. We have ordered the galaxies from top to bottom by increasing the distance modulus. As already observed in the F160W vs V-I plane, as the galaxy distance increase, the Cepheids location in the CMD moves to bluer colours and brighter magnitudes. A similar trend for the Cepheid brightness is noted in the PL plane (right panel of Fig.7). For comparison, we have over-plotted the blue boundary of the fundamental IS for  $Z = 0.008$  (LMC-like) and the red boundary for  $Z = 0.02$  (solar-like) to take into account a possible metallicity spread found in some of these galaxies (Bresolin 2011). In this plane, the agreement between theory and observations improves thanks to a smaller dependence on reddening and uncertainties in the colour-effective temperature transformations. In the case of NGC4258, when its metallicity spread is accounted for, the

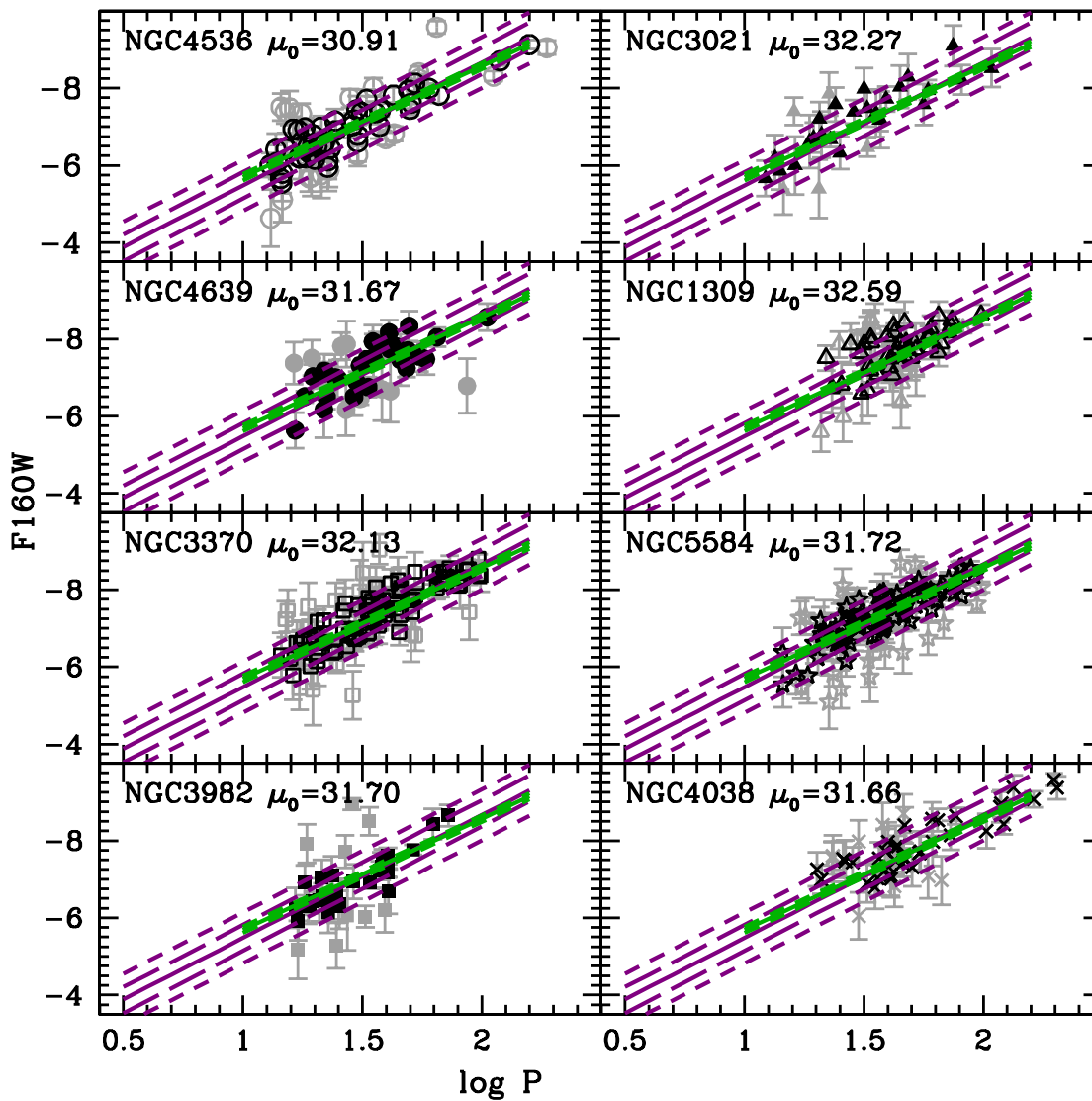


**Figure 6.** The same comparison as in Fig. 4 (right), for each galaxy of the sample. In this case, black and grey symbols represent good and rejected Cepheids as selected in Riess et al. (2011), respectively.

comparison with the predicted IS is satisfactory. The same holds for NGC3370, whereas the other two galaxies show a Cepheid distribution that is significantly bluer than predicted, even taking into account a possible revision of their metal abundance toward  $Z \sim 0.01$  as suggested by Bresolin (2011).

There is currently no clear explanation in the literature for the blue shift observed in distant galaxies, as well as for the very large color spread displayed by all the investigated samples (see also Tammann & Reindl 2012, for a discussion). A possible contribution to this trend could be given by a blending effect with faint unresolved companion stars that is expected to increase with the galaxy distance.

## 6 NEW DISTANCES AND THEIR IMPACT ON $H_0$

In this section, we derive new distance moduli for the galaxies of the sample using our set of pulsation models. Although the use of the Wesenheit relation is very common to derive the distance moduli and usually provides smaller errors than multi-wavelength PL both from observational and theoretical point of view, due to the discussed  $V - I$  uncertainties in these HST data, we prefer to use a pure NIR F160W–PL relation.

In particular, we adopt the following theoretical F160W PL for  $Z=0.02$  ( $Y=0.28$ ) and  $\log P > 1.0$ , given the period range available for distant galaxies.

$$F160W = -(2.81 \pm 0.08) - (2.88 \pm 0.01)\log P \quad (1)$$

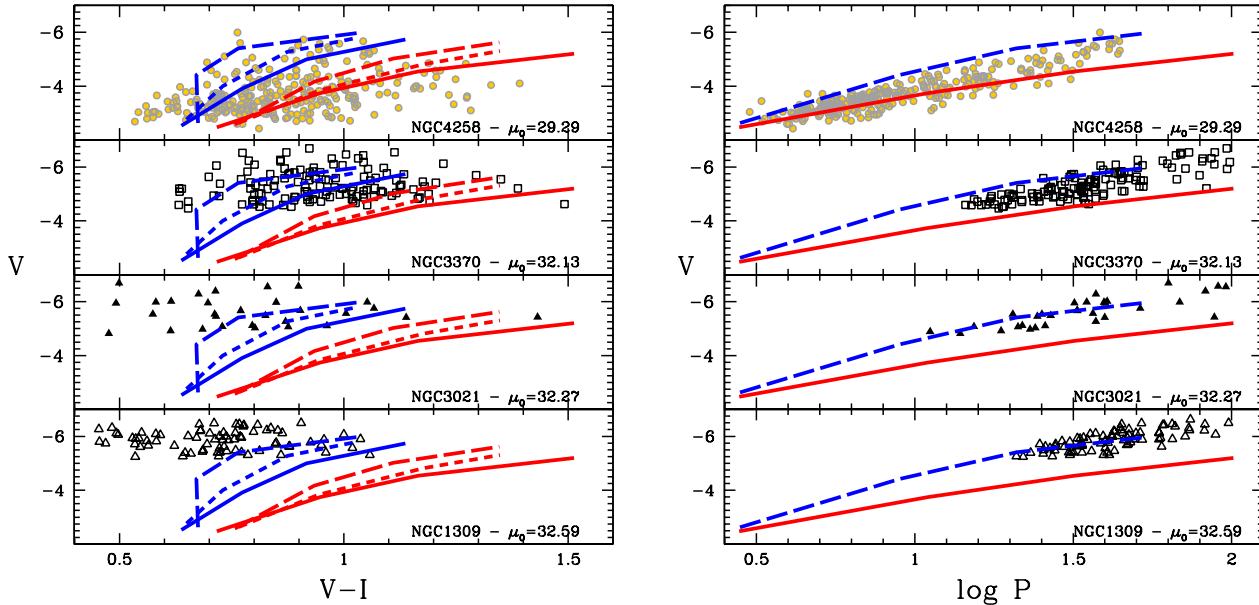


**Figure 7.** –*Left*– Comparison between the observed magnitude–colour distribution (V, V–I). The theoretical boundaries of the pulsation Instability Strip are plotted for the same chemical compositions chosen in Figs. 5–6 as well as the same symbols for each galaxy are used. –*Right*– The V Period–Luminosity distribution compared with theoretical prediction. For comparison, we have over–plotted the blue boundary of the IS for  $Z = 0.008$  (LMC–like) and the red boundary for  $Z = 0.02$  (solar–like).

The corresponding coefficients are also highlighted in bold–face in Table 2 and taking into account the small slope difference between the theoretical F160W PL (for  $Z=0.02$  and  $Y=0.28$  and  $\log P > 1$ ) and the one by Riess et al. (2011), we adopt their selection of *good* Cepheids.

As a first check, we applied our theoretical relation to the *good* Cepheids with  $\log P > 1$  in NGC4258 finding  $\mu_0 = 29.345 \pm 0.004$  mag with a  $\sigma = 0.34$  mag, which is in very good agreement with the maser distance:  $\mu_0 = 29.29^{+0.14}_{-0.16}$  mag.

Then, we applied the same relation to the *good* Cepheids of the other galaxies, obtaining the individual Cepheid distance moduli and the resulting mean values, as plotted in Fig. 8 and listed in column 7 of Table 4. These values are derived adopting a reddening correction (Schlafly & Finkbeiner 2011) but without assuming any metallicity dependence. As shown in Fig. 8, the Cepheid distribution around the derived mean distance modulus for each galaxy has a quite large scatter ( $\sigma \gtrsim 0.5$  mag). However, if we follow the same approach adopted by Riess et al. (2011), considering the large number of Cepheids observed in each galaxy, we derive a much smaller final uncertainty (standard error of the mean) for each mean distance modulus. In Fig. 9, we show the comparison between our derived mean distance moduli and the ones by Riess et al. (2011). The error-bars are relatively small because they represent the standard errors of the means and according to them we note a small discrepancy at the longest distance moduli. However, the agreement is well within  $1-\sigma$  over the whole distance range (see also Table 4).

On the basis of these distance moduli, we can compute the Hubble constant using the following equation:

$$\log H_{0,i} = \frac{(m_{v,i}^0 + 5a_v) - \mu_{0,i} + 25}{5} \quad (2)$$

where the quantities  $m_{v,i}^0 + 5a_v$  in Table 4, column 4, have been taken by Riess et al. (2011).

We find  $H_0 = 76.0 \pm 1.9$  km s<sup>−1</sup> Mpc<sup>−1</sup> ( $\sigma = 4.8$ ) in very good agreement within the errors with  $74.8 \pm 3.0$  km s<sup>−1</sup> Mpc<sup>−1</sup> found by Riess et al. (2011) on the basis of a metal dependent Wesenheit relation, but also with their best estimation  $73.8 \pm 2.3$  km s<sup>−1</sup> Mpc<sup>−1</sup> obtained taking into account different distance scale calibrations and different error sources. Finally, our result is also in good agreement with a completely independent estimation of the Hubble constant recently released by Freedman et al. (2012) that uses the Spitzer calibration to the Key Project sample of Cepheids, i.e.  $H_0 = 74.3 \pm 2.1$  (systematic) km s<sup>−1</sup> Mpc<sup>−1</sup>.

## 7 CONCLUSIONS

In this paper we present the predictions of our nonlinear, nonlocal and time–dependent pulsation scenario for Classical Cepheids transformed into the WFC3@HST filters, as a unique theoretical tool to study the properties of new and future observations with this powerful camera. We have analysed the metallicity effect on the Cepheid PL relation in these photometric bands and confirmed the result already obtained in the Johnson–Cousin photometric system, that the metallicity effect decreases when increasing the wavelength (from F555W to F160W). In particular, the use of a NIR F160W PL relation provides an accuracy of few percent when the correct metallicity reference sample is adopted.

Our model predictions are useful to investigate the properties of Cepheids observed in these filters in 8 distant galaxies hosting SNIa that have been recently used to



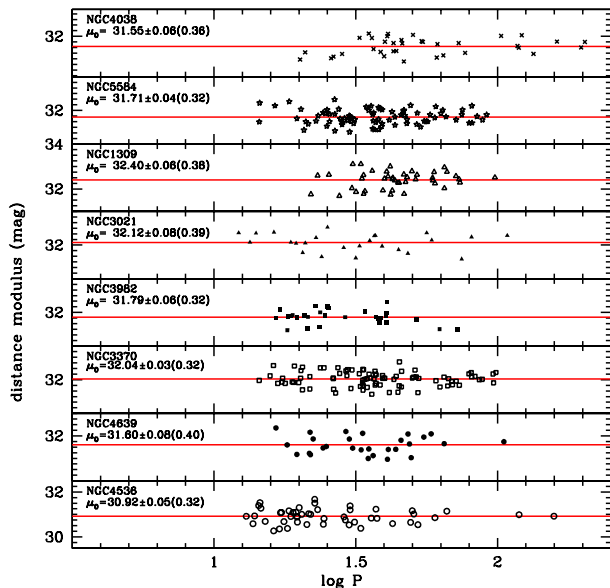


**Figure 8.** Individual Cepheid distance moduli obtained with the theoretical F160W PL relation for  $Z=0.02$ ,  $Y=0.28$  and  $\log P > 1$ . In each panel, the solid line represents the inferred mean value.

estimate the Hubble constant  $H_0$ . We find a satisfactory agreement between observed and predicted Cepheid properties, with the exception of pulsators in NGC1309, NGC3021 and NGC3370 that appear significantly brighter and bluer than Cepheid models. This effect has already been previously noted by Tammann & Reindl (2012) on the basis of a comparison of these Cepheid samples with the Galactic one and could be related to the increasing crowding effect at larger distances (Stetson et al. 1998; Chavez et al. 2012).

We have applied the theoretical F160W PL relation for the chemical composition currently adopted for NGC 4258 ( $Z=0.02$ ;  $Y=0.28$ ) and  $\log P > 1$  to derive new individual and average distance moduli for the investigated Cepheid samples. The resulting Hubble constant is  $H_0 = 76.0 \pm 1.9$   $\text{km s}^{-1} \text{Mpc}^{-1}$  ( $\sigma = 4.8$ ), in excellent agreement with the values obtained by Riess et al. (2011) and Freedman et al. (2012). This agreement suggests that adopting a very simple and direct approach, based on the predictions of non-linear pulsation models, we are able to constrain the extragalactic distance scale and the Hubble constant at the same level of accuracy obtained from an observational point of view.

## ACKNOWLEDGMENTS

The authors warmly thanks Santi Cassisi and Adriano Pietrinferri for kindly providing the updated bolometric corrections in WFC3/HST bands for both UVIS and IR channels. GF has been supported by the INAF fellowship 2009 grant and by the COSMIC-LAB ERC grant (under contract ERC-2010-AdG-267675). We thank the referee V. Scowcroft for her suggestions/comments that improved the readability and the impact of this paper.

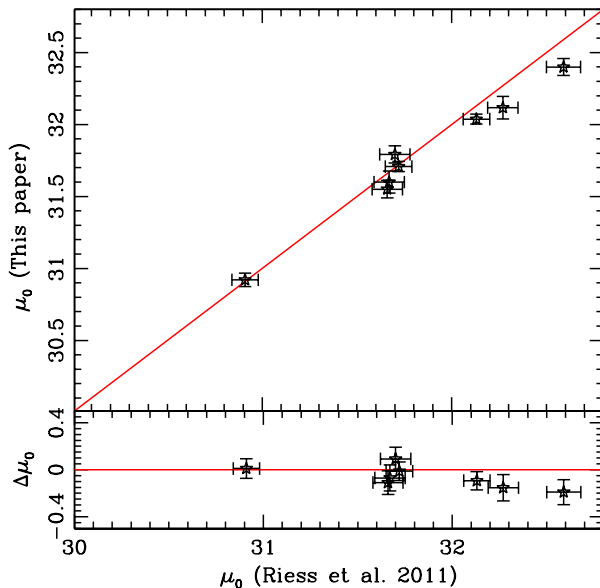


**Figure 9.** –*Top panel*– Comparison between the distance modulus found by Riess et al. (2011) using a metal dependent Wesenheit relation and the one derived in this paper using our theoretical F160W PL for  $Z=0.02$ – $Y=0.28$  and for periods larger than 10 days. –*Bottom panel*– Difference of the distance moduli as a function the distance modulus found by Riess et al. (2011).

## REFERENCES

- Bono, G., Caputo, F., Castellani, V., & Marconi, M. 1999a, *ApJ*, 512, 711  
 Bono, G., Caputo, F., Fiorentino, G., Marconi, M., & Musella, I. 2008, *ApJ*, 684, 102  
 Bono, G., Caputo, F., Marconi, M., & Musella, I. 2010, *ApJ*, 715, 277  
 Bono, G., Castellani, V., & Marconi, M. 2000, *ApJ*, 529, 293  
 Bono, G., Marconi, M., & Stellingwerf, R. F. 1999b, *ApJS*, 122, 167  
 Bresolin, F. 2011, *ApJ*, 729, 56  
 Caputo, F., Castellani, V., Marconi, M., & Ripepi, V. 2000, *MNRAS*, 316, 819  
 Caputo, F., Marconi, M., & Musella, I. 2002, *ApJ*, 566, 833  
 Cardelli, J., Clayton, G., & Mathis, J. 1989, *ApJ*, 345, 245  
 Chavez, J. M., Macri, L. M., & Pellerin, A. 2012, *AJ*, 144, 113  
 Fiorentino, G., Caputo, F., Marconi, M., & Musella, I. 2002, *ApJ*, 576, 402  
 Fiorentino, G., Marconi, M., Musella, I., & Caputo, F. 2007, *A&A*, 476, 863  
 Fiorentino, G., Tolstoy, E., Diolaiti, E., Valenti, E., Cignoni, M., & Mackey, A. D. 2011, *A&A*, 535, A63  
 Fiorentino, G., et al. 2010, *ApJ*, 711, 808  
 —. 2012, *Ap&SS*, 100  
 Freedman, W. L., & Madore, B. F. 2010, *ARA&A*, 48, 673  
 Freedman, W. L., Madore, B. F., Scowcroft, V., Burns, C., Monson, A., Persson, S. E., Seibert, M., & Rigby, J. 2012, *ApJ*, 758, 24  
 Freedman, W. L., et al. 2001, *ApJ*, 553, 47

**Table 1.** Linear PL relations in HST/WFC3 photometric system for a selected sample of filters. Other filters are available upon request.

Z	Y	$\alpha$	$\beta$
F555W = $\alpha + \beta \log P$			
0.0004	0.24	-1.09 ± 0.23	-2.99 ± 0.01
0.004	0.25	-1.45 ± 0.21	-2.70 ± 0.02
0.008	0.25	-1.48 ± 0.22	-2.52 ± 0.02
0.01	0.26	-1.33 ± 0.27	-2.59 ± 0.02
0.02	0.25	-1.32 ± 0.21	-2.42 ± 0.02
0.02	0.26	-1.29 ± 0.21	-2.60 ± 0.02
0.02	0.28	-1.67 ± 0.17	-2.08 ± 0.01
0.02	0.31	-1.54 ± 0.19	-2.33 ± 0.02
0.03	0.275	-1.34 ± 0.19	-2.27 ± 0.02
0.03	0.31	-1.56 ± 0.19	-2.00 ± 0.01
0.03	0.335	-1.49 ± 0.15	-2.11 ± 0.01
0.04	0.25	-1.22 ± 0.16	-2.32 ± 0.01
0.04	0.29	-1.46 ± 0.14	-2.10 ± 0.01
0.04	0.33	-1.40 ± 0.11	-2.15 ± 0.01
F606W = $\alpha + \beta \log P$			
0.0004	0.24	-1.25 ± 0.20	-3.07 ± 0.01
0.004	0.25	-1.62 ± 0.19	-2.79 ± 0.02
0.008	0.25	-1.65 ± 0.20	-2.63 ± 0.02
0.01	0.26	-1.50 ± 0.24	-2.70 ± 0.02
0.02	0.25	-1.50 ± 0.19	-2.54 ± 0.02
0.02	0.26	-1.48 ± 0.19	-2.71 ± 0.02
0.02	0.28	-1.82 ± 0.16	-2.23 ± 0.01
0.02	0.31	-1.69 ± 0.17	-2.46 ± 0.01
0.03	0.275	-1.54 ± 0.17	-2.41 ± 0.01
0.03	0.31	-1.73 ± 0.17	-2.16 ± 0.01
0.03	0.335	-1.65 ± 0.14	-2.28 ± 0.01
0.04	0.25	-1.43 ± 0.15	-2.46 ± 0.01
0.04	0.29	-1.65 ± 0.13	-2.25 ± 0.01
0.04	0.33	-1.59 ± 0.10	-2.30 ± 0.01
F814W = $\alpha + \beta \log P$			
0.0004	0.24	-1.68 ± 0.16	-3.23 ± 0.01
0.004	0.25	-2.04 ± 0.15	-2.96 ± 0.01
0.008	0.25	-2.07 ± 0.15	-2.83 ± 0.01
0.01	0.26	-1.93 ± 0.19	-2.91 ± 0.02
0.02	0.25	-1.96 ± 0.15	-2.77 ± 0.01
0.02	0.26	-1.93 ± 0.15	-2.91 ± 0.01
0.02	0.28	-2.20 ± 0.12	-2.50 ± 0.01
0.02	0.31	-2.08 ± 0.14	-2.71 ± 0.01
0.03	0.275	-2.00 ± 0.14	-2.65 ± 0.01
0.03	0.31	-2.13 ± 0.13	-2.46 ± 0.01
0.03	0.335	-2.04 ± 0.11	-2.58 ± 0.01
0.04	0.25	-1.90 ± 0.12	-2.72 ± 0.01
0.04	0.29	-2.10 ± 0.11	-2.53 ± 0.01
0.04	0.33	-2.02 ± 0.08	-2.57 ± 0.01
F160W = $\alpha + \beta \log P$			
0.0004	0.24	-2.31 ± 0.09	-3.454 ± 0.005
0.004	0.25	-2.63 ± 0.08	-3.224 ± 0.007
0.008	0.25	-2.62 ± 0.08	-3.153 ± 0.006
0.01	0.26	-2.50 ± 0.10	-3.258 ± 0.009
0.02	0.25	-2.53 ± 0.08	-3.179 ± 0.007
0.02	0.26	-2.52 ± 0.08	-3.258 ± 0.007
0.02	0.28	-2.67 ± 0.06	-2.977 ± 0.004
0.02	0.31	-2.56 ± 0.07	-3.139 ± 0.006
0.03	0.275	-2.57 ± 0.09	-3.089 ± 0.007
0.03	0.31	-2.60 ± 0.07	-2.995 ± 0.005
0.03	0.335	-2.48 ± 0.06	-3.111 ± 0.005
0.04	0.25	-2.48 ± 0.06	-3.173 ± 0.005
0.04	0.29	-2.64 ± 0.07	-2.995 ± 0.005
0.04	0.33	-2.64 ± 0.07	-2.995 ± 0.005

**Table 2.** As in Table 1, but for quadratic (left) and broken linear (right) PL-relations

Z	Y	$\alpha$	$\beta$	$\gamma$	$\alpha_{\log P \leq 1}$	$\beta_{\log P \leq 1}$	$\alpha_{\log P > 1}$	$\beta_{\log P > 1}$	
F555W = $\alpha + \beta \log P + \gamma \log P^2$					F555W = $\alpha + \beta \log P$				
0.0004	0.24	-1.01±0.23	-3.17± 0.07	0.09±0.03	-1.10± 0.20	-2.96±0.03	-1.29± 0.28	-2.85± 0.04	
0.004	0.25	-0.56±0.18	-4.65± 0.09	0.93±0.04	-1.09± 0.14	-3.20±0.03	-2.31± 0.26	-2.06± 0.06	
0.008	0.25	-0.72±0.19	-4.19± 0.09	0.79±0.04	-1.17± 0.16	-2.95±0.04	-2.27± 0.26	-1.94± 0.06	
0.01	0.26	-0.35±0.25	-4.71± 0.14	1.03±0.07	-0.99± 0.20	-3.05±0.05	-2.20± 0.33	-1.93± 0.08	
0.02	0.25	-0.96±0.20	-3.28± 0.10	0.45±0.05	-1.18± 0.17	-2.63±0.03	-1.73± 0.27	-2.08± 0.08	
0.02	0.26	-0.73±0.20	-3.96± 0.10	0.72±0.05	-1.12± 0.15	-2.86±0.03	-2.16± 0.29	-1.92± 0.09	
0.02	0.28	-1.31±0.16	-2.88± 0.06	0.38±0.03	-1.52± 0.11	-2.29±0.02	-2.06± 0.23	-1.80± 0.04	
0.02	0.31	-1.10±0.19	-3.27± 0.10	0.45±0.05	-1.41± 0.15	-2.49±0.04	-1.98± 0.24	-2.00± 0.05	
0.03	0.275	-1.11±0.19	-2.81± 0.09	0.28±0.04	-1.29± 0.16	-2.33±0.03	-1.76± 0.22	-1.95± 0.05	
0.03	0.31	-1.27±0.19	-2.63± 0.09	0.30±0.04	-1.47± 0.16	-2.12±0.04	-1.86± 0.23	-1.78± 0.04	
0.03	0.335	-1.00±0.14	-3.13± 0.07	0.46±0.03	-1.30± 0.10	-2.36±0.03	-1.86± 0.18	-1.84± 0.03	
0.04	0.25	-1.13±0.16	-2.56± 0.07	0.14±0.04	-1.19± 0.14	-2.35±0.02	-1.53± 0.20	-2.08± 0.07	
0.04	0.29	-1.26±0.14	-2.60± 0.06	0.26±0.03	-1.40± 0.12	-2.20±0.02	-1.86± 0.17	-1.80± 0.04	
0.04	0.33	-1.09±0.10	-2.82± 0.05	0.32±0.02	-1.29± 0.08	-2.29±0.02	-1.72± 0.13	-1.92± 0.03	
F606W = $\alpha + \beta \log P + \gamma \log P^2$					F606W = $\alpha + \beta \log P$				
0.0004	0.24	-1.19± 0.20	-3.20± 0.07	0.06± 0.03	-1.27± 0.18	-3.03± 0.03	-1.42± 0.25	-2.95± 0.04	
0.004	0.25	-0.82± 0.17	-4.53± 0.08	0.83± 0.04	-1.29± 0.13	-3.24± 0.03	-2.38± 0.24	-2.22± 0.05	
0.008	0.25	-0.96± 0.17	-4.12± 0.08	0.71± 0.04	-1.37± 0.14	-3.01± 0.03	-2.35± 0.24	-2.11± 0.05	
0.01	0.26	-0.62± 0.22	-4.61± 0.13	0.93± 0.06	-1.20± 0.18	-3.12± 0.05	-2.29± 0.30	-2.10± 0.07	
0.02	0.25	-1.18± 0.18	-3.33± 0.09	0.41± 0.05	-1.38± 0.15	-2.74± 0.03	-1.89± 0.25	-2.24± 0.07	
0.02	0.26	-0.98± 0.18	-3.94± 0.09	0.65± 0.05	-1.33± 0.14	-2.94± 0.03	-2.26± 0.26	-2.09± 0.08	
0.02	0.28	-1.49± 0.15	-2.96± 0.06	0.35± 0.03	-1.69± 0.10	-2.42± 0.02	-2.18± 0.21	-1.97± 0.04	
0.02	0.31	-1.29± 0.17	-3.32± 0.09	0.41± 0.04	-1.58± 0.13	-2.61± 0.03	-2.10± 0.22	-2.16± 0.05	
0.03	0.275	-1.32± 0.17	-2.92± 0.08	0.26± 0.04	-1.49± 0.15	-2.47± 0.03	-1.93± 0.21	-2.11± 0.05	
0.03	0.31	-1.45± 0.17	-2.76± 0.08	0.28± 0.04	-1.64± 0.14	-2.23± 0.03	-2.01± 0.20	-1.96± 0.04	
0.03	0.335	-1.19± 0.12	-3.22± 0.06	0.43± 0.03	-1.47± 0.09	-2.51± 0.02	-2.00± 0.17	-2.03± 0.03	
0.04	0.25	-1.34± 0.15	-2.70± 0.07	0.13± 0.04	-1.40± 0.13	-2.50± 0.02	-1.71± 0.18	-2.23± 0.06	
0.04	0.29	-1.46± 0.13	-2.73± 0.05	0.24± 0.03	-1.59± 0.11	-2.34± 0.02	-2.04± 0.16	-1.97± 0.04	
0.04	0.33	-1.30± 0.09	-2.93± 0.04	0.29± 0.02	-1.49± 0.07	-2.43± 0.02	-1.88± 0.12	-2.09± 0.02	
F814W = $\alpha + \beta \log P + \gamma \log P^2$					F814W = $\alpha + \beta \log P$				
0.0004	0.24	-1.66± 0.16	-3.28±0.05	0.03± 0.02	-1.70± 0.14	-3.19±0.02	-1.79± 0.19	-3.15± 0.03	
0.004	0.25	-1.42± 0.13	-4.31±0.06	0.65± 0.03	-1.79± 0.10	-3.31±0.02	-2.63± 0.18	-2.52± 0.04	
0.008	0.25	-1.52± 0.14	-4.02±0.06	0.57± 0.03	-1.85± 0.11	-3.13±0.02	-2.63± 0.19	-2.41± 0.04	
0.01	0.26	-1.22± 0.18	-4.44±0.10	0.74± 0.05	-1.69± 0.14	-3.24±0.04	-2.56± 0.24	-2.43± 0.06	
0.02	0.25	-1.69± 0.15	-3.41±0.07	0.34± 0.04	-1.85± 0.12	-2.93±0.02	-2.26± 0.20	-2.52± 0.06	
0.02	0.26	-1.52± 0.14	-3.91±0.08	0.53± 0.04	-1.81± 0.11	-3.10±0.02	-2.55± 0.21	-2.41± 0.06	
0.02	0.28	-1.94± 0.12	-3.09±0.04	0.28± 0.02	-2.09± 0.08	-2.66±0.02	-2.50± 0.16	-2.29± 0.03	
0.02	0.31	-1.75± 0.13	-3.42±0.07	0.34± 0.03	-1.98± 0.10	-2.84±0.02	-2.42± 0.17	-2.46± 0.04	
0.03	0.275	-1.82± 0.14	-3.07±0.07	0.21± 0.03	-1.96± 0.12	-2.70±0.03	-2.32± 0.17	-2.41± 0.04	
0.03	0.31	-1.92± 0.13	-2.90±0.06	0.21± 0.03	-2.06± 0.11	-2.56±0.03	-2.33± 0.16	-2.31± 0.03	
0.03	0.335	-1.68± 0.10	-3.30±0.05	0.33± 0.02	-1.89± 0.07	-2.77±0.02	-2.30± 0.13	-2.39± 0.03	
0.04	0.25	-1.82± 0.12	-2.91±0.05	0.11± 0.03	-1.87± 0.10	-2.75±0.02	-2.11± 0.15	-2.55± 0.05	
0.04	0.29	-1.95± 0.11	-2.89±0.04	0.19± 0.02	-2.05± 0.09	-2.60±0.02	-2.39± 0.13	-2.31± 0.03	
0.04	0.33	-1.80± 0.07	-3.04±0.03	0.22± 0.02	-1.94± 0.06	-2.67±0.01	-2.25± 0.09	-2.40± 0.02	
F160W = $\alpha + \beta \log P + \gamma \log P^2$					F160W = $\alpha + \beta \log P$				
0.0004	0.24	-2.30± 0.09	-3.47± 0.03	0.01± 0.01	-2.33±0.08	-3.43± 0.01	-2.37± 0.10	-3.42±0.02	
0.004	0.25	-2.31± 0.07	-3.92± 0.03	0.33± 0.02	-2.50±0.05	-3.40± 0.01	-2.93± 0.10	-3.00±0.02	
0.008	0.25	-2.34± 0.07	-3.76± 0.03	0.29± 0.02	-2.51±0.06	-3.31± 0.01	-2.91± 0.10	-2.94±0.02	
0.01	0.26	-2.13± 0.09	-4.06± 0.05	0.39± 0.03	-2.37±0.08	-3.43± 0.02	-2.83± 0.13	-3.01±0.03	
0.02	0.25	-2.40± 0.08	-3.50± 0.04	0.17± 0.02	-2.48±0.06	-3.26± 0.01	-2.69± 0.11	-3.05±0.03	
0.02	0.26	-2.30± 0.08	-3.78± 0.04	0.28± 0.02	-2.45±0.06	-3.35± 0.01	-2.85± 0.11	-3.00±0.03	
0.02	0.28	-2.54± 0.06	-3.26± 0.02	0.13± 0.01	-2.62±0.04	-3.05± 0.01	<b>-2.81± 0.08</b>	<b>-2.88±0.01</b>	
0.02	0.31	-2.39± 0.07	-3.50± 0.04	0.18± 0.02	-2.51±0.05	-3.20± 0.01	-2.73± 0.09	-3.01±0.02	
0.03	0.275	-2.48± 0.09	-3.30± 0.04	0.11± 0.02	-2.55±0.08	-3.11± 0.02	-2.74± 0.10	-2.96±0.02	
0.03	0.31	-2.51± 0.07	-3.18± 0.03	0.09± 0.01	-2.57±0.06	-3.03± 0.01	-2.68± 0.08	-2.93±0.02	
0.03	0.335	-2.31± 0.05	-3.45± 0.03	0.16± 0.01	-2.41±0.04	-3.20± 0.01	-2.60± 0.07	-3.02±0.01	
0.04	0.25	-2.45± 0.06	-3.24± 0.03	0.04± 0.02	-2.47±0.06	-3.18± 0.01	-2.57± 0.08	-3.10±0.03	
0.04	0.29	-2.57± 0.07	-3.17± 0.03	0.09± 0.01	-2.62±0.06	-3.02± 0.01	-2.70± 0.08	-3.00±0.02	

**Table 3.** Wesenheit–relation for different chemical compositions.

Z	Y	$\alpha$	$\beta$
F555W-2.42(F555W-F814W)		$=\alpha + \beta \log P$	
0.0004	0.24	-2.53± 0.06	-3.563± 0.004
0.004	0.25	-2.87± 0.06	-3.329± 0.006
0.008	0.25	-2.89± 0.06	-3.260± 0.005
0.01	0.26	-2.79± 0.08	-3.359± 0.008
0.02	0.25	-2.87± 0.07	-3.275± 0.006
0.02	0.26	-2.84± 0.07	-3.352± 0.006
0.02	0.28	-2.97± 0.05	-3.096± 0.003
0.02	0.31	-2.86± 0.06	-3.254± 0.005
0.03	0.275	-2.93± 0.08	-3.196± 0.006
0.03	0.31	-2.94± 0.06	-3.125± 0.004
0.03	0.335	-2.81± 0.05	-3.240± 0.004
0.04	0.25	-2.85± 0.05	-3.291± 0.004
0.04	0.29	-3.01± 0.06	-3.128± 0.005
0.04	0.33	-2.91± 0.03	-3.155± 0.003
F606W-2.82(F606W-F814W)		$=\alpha + \beta \log P$	
0.0004	0.24	-2.47± 0.07	-3.518± 0.004
0.004	0.25	-2.81± 0.07	-3.273± 0.006
0.008	0.25	-2.83± 0.08	-3.190± 0.006
0.01	0.26	-2.72± 0.10	-3.285± 0.009
0.02	0.25	-2.78± 0.08	-3.186± 0.007
0.02	0.26	-2.76± 0.08	-3.273± 0.007
0.02	0.28	-2.91± 0.06	-2.994± 0.004
0.02	0.31	-2.79± 0.07	-3.158± 0.006
0.03	0.275	-2.83± 0.09	-3.098± 0.007
0.03	0.31	-2.86± 0.07	-3.013± 0.005
0.03	0.335	-2.74± 0.06	-3.127± 0.005
0.04	0.25	-2.75± 0.06	-3.188± 0.005
0.04	0.29	-2.91± 0.07	-3.022± 0.005
0.04	0.33	-2.81± 0.04	-3.050± 0.003
F160W-0.41(V-I)		$=\alpha + \beta \log P$	
0.0004	0.24	-2.54± 0.06	-3.540± 0.004
0.004	0.25	-2.85± 0.05	-3.320± 0.006
0.008	0.25	-2.84± 0.06	-3.271± 0.004
0.01	0.26	-2.73± 0.07	-3.382± 0.007
0.02	0.25	-2.78± 0.06	-3.315± 0.005
0.02	0.26	-2.76± 0.06	-3.376± 0.005
0.02	0.28	-2.87± 0.04	-3.138± 0.003
0.02	0.31	-2.76± 0.05	-3.285± 0.004
0.03	0.275	-2.81± 0.07	-3.243± 0.006
0.03	0.31	-2.81± 0.05	-3.182± 0.004
0.03	0.335	-2.69± 0.04	-3.299± 0.003
0.04	0.25	-2.74± 0.04	-3.340± 0.004
0.04	0.29	-2.89± 0.05	-3.181± 0.004
0.04	0.33	-2.78± 0.03	-3.208± 0.002

Haschke, R., Grebel, E. K., & Duffau, S. 2012, *AJ*, 144, 106

Herrnstein, J. R., Moran, J. M., Greenhill, L. J., & Trotter, A. S. 2005, *ApJ*, 629, 719

Inno, L., et al. 2013, *ApJ*, 764, 84

Kennicutt, Jr., R. C., et al. 1998, *ApJ*, 498, 181

Laney, C. D., Joner, M. D., & Pietrzyński, G. 2012, *MNRAS*, 419, 1637

Macri, L. M., Stanek, K. Z., Bersier, D., Greenhill, L. J., & Reid, M. J. 2006, *ApJ*, 652, 1133

Madore, B. F. 1976, in *Royal Greenwich Observatory Bulletins*, Vol. 182, *The Galaxy and the Local Group*, ed. R. J. Dickens, J. E. Perry, F. G. Smith, & I. R. King, 153

Marconi, M., Molinaro, R., Ripepi, V., Musella, I., & Brocato, E. 2012, *ArXiv e-prints*

Marconi, M., Musella, I., & Fiorentino, G. 2005, *ApJ*, 632, 590

Marconi, M., et al. 2010, *ApJ*, 713, 615

Ngeow, C.-C., Kanbur, S. M., Nikolaev, S., Buonaccorsi, J., Cook, K. H., & Welch, D. L. 2005, *MNRAS*, 363, 831

**Table 4.** Global properties of the SNIa host galaxies observed with WFC3@HST (see text for details).

ID	$N_{\text{Cep}}(\text{tot}/\text{good})$	$< 12 + \log[\text{O}/\text{H}] >$	$m_{\text{v},i}^0 + 5a_{\text{v}}$	$\mu_0(\text{Riess})$	$\mu_0(\text{this paper})$	$A_{\text{V}}$	$A_{\text{I}}$	$A_{\text{F160W}}$
NGC 4258	167/117	$8.89^a \pm 0.09$		29.29	$29.345 \pm 0.004^b(0.34)$	0.044	0.024	0.009
NGC 4536	69/49	$8.77^a \pm 0.14$	15.147	$30.91 \pm 0.07$	$30.92 \pm 0.05^b(0.32)$	0.050	0.027	0.010
NGC 4639	37/25	$8.98^a \pm 0.15$	16.040	$31.67 \pm 0.08$	$31.60 \pm 0.08^b(0.40)$	0.071	0.039	0.015
NGC 3370	101/69	$8.81^a \pm 0.14$	16.545	$32.13 \pm 0.07$	$32.04 \pm 0.03^b(0.32)$	0.084	0.046	0.018
NGC 3982	38/22	$8.77^a \pm 0.24$	15.953	$31.70 \pm 0.08$	$31.79 \pm 0.06^b(0.32)$	0.039	0.021	0.008
NGC 3021	30/22	$8.89^a \pm 0.18$	16.699	$32.27 \pm 0.08$	$32.12 \pm 0.08^b(0.39)$	0.037	0.020	0.008
NGC 1309	56/30	$8.90^a \pm 0.14$	16.768	$32.59 \pm 0.09$	$32.40 \pm 0.06^b(0.38)$	0.109	0.060	0.023
NGC 5584	103/78	$8.84^a \pm 0.12$	16.274	$31.72 \pm 0.07$	$31.71 \pm 0.04^b(0.32)$	0.107	0.058	0.022
NGC 4038	46/32	$9.01^a \pm 0.09$	15.901	$31.66 \pm 0.08$	$31.55 \pm 0.06^b(0.36)$	0.127	0.070	0.008

<sup>a</sup> Metallicity content from Riess et al. (2011);

<sup>b</sup>These errors have been computed using the standard deviation  $\sigma$  (in parenthesis) of  $\langle \mu_0 \rangle$  divided by  $\sqrt{N_{\text{Cep}}(\text{tot})}$ , see Fig. 7.

- Ngeow, C.-C., Kanbur, S. M., Bellinger, E. P., Marconi, M., Musella, I., Cignoni, M., & Lin, Y.-H. 2012, *A&A*, 341, 105
- Monson, A. J., Freedman, W. L., Madore, B. F., Persson, S. E., Scowcroft, V., Seibert, M., & Rigby, J. R. 2012, *ApJ*, 759, 146
- Riess, A. G., et al. 2009a, *ApJ*, 699, 539
- . 2009b, *ApJs*, 183, 109
- . 2011, *ApJ*, 730, 119
- Ripepi, V., et al. 2012, *MNRAS*, 424, 1807
- Romaniello, M., et al. 2008, *A&A*, 488, 731
- Sakai, S., Ferrarese, L., Kennicutt, Jr., R. C., & Saha, A. 2004, *ApJ*, 608, 42
- Schlafly, E. F., & Finkbeiner, D. P. 2011, *ApJ*, 737, 103
- Scowcroft, V., Freedman, W. L., Madore, B. F., Monson, A. J., Persson, S. E., Seibert, M., Rigby, J. R., & Sturch, L. 2011, *ApJ*, 743, 76
- Soszyński, I., Gieren, W., & Pietrzyński, G. 2005, *PASP*, 117, 823
- Soszyński, I., et al. 2008, *AcA*, 58, 163
- Stellingwerf, R. F. 1978, *ApJ*, 224, 953
- Stetson, P. B., et al. 1998, *ApJ*, 508, 491
- Tammann, G. A., & Reindl, B. 2012, *Ap&SS*, 341, 3
- Tammann, G. A., Sandage, A., & Reindl, B. 2003, *A&A*, 404, 423
- Walker, A. R. 2012, *Ap&SS*, 341, 43